2016

R134a Flow Boiling Heat transfer on an Electrically Heated Carbon/Carbon Surface

Luca Doretti
Dept. of Civil, Architectural and Environmental Engineering, University of Padova, Italy, luca.doretti@unipd.it

Simone Mancin
Dept. of Management and Engineering, University of Padova, Italy, simone.mancin@unipd.it

Claudio Zilio
Dept. of Management and Engineering, University of Padova, Italy, claudio.zilio@unipd.it

Giovanni A. Longo
Dept. of Management and Engineering, University of Padova, Italy, tony@gest.unipd.it

R134a Flow Boiling Heat transfer on an Electrically Heated Carbon/Carbon Surface

Luca DORETTI[1], Simone MANCIN[2*], Claudio ZILIO[2], Giovanni A. LONGO[2]

[1] Dept. of Civil, Architectural and Environmental Engineering
University of Padova, Via Venezia, 1 PADOVA - 35131, Italy
luca.doretti@unipd.it
[2] Dept. of Management and Engineering
University of Padova, Str.lla S. Nicola, 1, VICENZA - 36100, Italy
simone.mancin@unipd.it, claudio.zilio@unipd.it, tony@gest.unipd.it
*Corresponding Author

ABSTRACT

This paper presents the experimental measurements carried out during flow boiling heat transfer of R134a on a Carbon/Carbon surface. This material appears to be a viable option for future thermal management devices because it exploits interesting properties having a low density and a relatively high thermal conductivity as compared to copper; moreover, it is already used in many industrial applications where it is shaped in various forms even complex. The sample was tested in a new experimental facility especially designed to study the flow boiling heat transfer process on innovative materials and enhanced micro- and nano-structured surfaces. The tests were run at constant saturation temperature of 30 °C and heat flux of 50 kW m^{-2}, by varying the refrigerant mass velocity from 50 to 200 kg m^{-2} s^{-1}.

1. INTRODUCTION

Since earlies 1960s, Carbon/Carbon (C/C) composite materials have been studied for several industrial applications related to noteworthy thermal and mechanical characteristics. They combine light weight, exceptional strength, and stiffness with excellent refractory properties, making them the material of choice for severe-environment applications, such as atmospheric reentry, solid rocket motor exhaust, and disk brakes in high performance military and commercial aircraft, high speed trains, and racing cars. Emerging areas of applications include biomedical devices, aero-engine components, heating elements with 2000 °C temperature, and hardware for metal forming and glass making. (C/C composite project, 2009-2012). Their development is limited by economical and technical constraints, both of them being critical (Rovillain *et al.*, 2001).

As the number of electrical and electronic systems increases, their physical sizes decrease, and the spacing between electrical components decreases, both the total amount of heat generated (hence to be dissipated) and the power density (the heat generated per unit volume) increase significantly. There is a general agreement in the scientific community that current air-cooling technologies are asymptotically approaching their limits imposed by available cooling area, available air flow rate, fan power, and noise. Boiling can be a very efficient heat transfer mechanism, thus it can be used to maintain the junction temperature of electronics equipment at values compatible with the technology using compact heat sinks. In the last decades, surface treatments, such as microporous coatings, Carbon Nano Tubes coatings, or micro- and nano-structured surfaces have been demonstrated to be very effective in enhancing the boiling performance. (Forrest *et al.*, 2010, Khanikar *et al*., 2009, Singh *et al.,* 2010, Chang *et al.*, 2010, Ammerman and You (2011), and Mancin *et al.*, 2015).

A possible alternative to the use of treated surfaces, may be represented by the adoption of textured composite materials. Carbon/Carbon composite materials are candidates for use in advanced thermal protection systems, as thermal shields but there are not any constrains in applying them as interface materials for advanced efficient heat spreader. In fact, having a low density and a tailored thermal conductivity, C/C composites could be used in replacement of heavy copper spreader to dissipate high heat fluxes while lowering the weight and volume of the heat sinks. For this reasons, this work investigates a novel and previously unexplored application of C/C materials as boiling surface for high heat flux dissipation. Thus, this paper presents the heat transfer measurements collected during flow boiling of R134a on an electrically heated C/C surface by varying the refrigerant mass velocity from 50 kg m^{-2} s^{-1} to 200 kg m^{-2} s^{-1} at an imposed heat flux of 50 kW m^{-2}, keeping constant the inlet saturation temperature at 30 °C.

2. EXPERIMENTAL APPARATUS

The experimental setup is located at the Nano Heat Transfer Lab (NHT-Lab) at the Department of Management and Engineering of the University of Padova. As shown in Figure 1, the experimental facility consists of three loops: refrigerant, cooling water, and hot water loops. The rig was designed for heat transfer and pressure drop measurements and flow visualization during either vaporization or condensation of pure refrigerants and refrigerants mixtures inside structured micro- and nano-geometries.

The refrigerant is pumped through the circuit by means of a magnetically coupled gear pump, then it is vaporized in a Brazed Plate Heat Exchanger (BPHE) fed with hot water to achieve the desired value of vapor quality. The hot water is supplied by a thermostatic bath; both water flow rate and water temperature can be independently set. The heat flow rate exchanged at the BPHE evaporator is accurately measured by means of a magnetic flow meter and a calibrated T-type thermopile; furthermore, preliminary tests were run to verify the heat balance between refrigerant and water sides, the results showed a misbalance always less than 2%.

The refrigerant enters the test section at a known mass velocity and vapor quality and then it is vaporized by the heat flow rate generated by a calibrated Ni-Cr wire resistance. The electrical power supplied to the sample is indirectly measured by means of a calibrated reference resistance (shunt) and by the measurement of the effective electrical difference potential of the resistance wire inserted in the copper heater. The current can be calculated from the Ohm's law. The fluid leaves the test section and enters in a post-condenser, a brazed plate heat exchanger fed with tap water, where it is fully condensed and subcooled. A damper connected to a compressed air line operates as pressure regulator to control the saturation conditions in the refrigerant loop. As shown in Figure 1, the refrigerant pressure and temperature are measured at several locations throughout the circuit to estimate the refrigerant properties at the inlet and outlet of each heat exchanger. The refrigerant mass flow rate can be independently controlled by the gear pump and it is measured by means of a Coriolis effect flowmeter. No oil circulates in the refrigerant loop. Furthermore, a high speed camera (Olympus, i-speed 3) was installed over the test section for boiling visualization. Table 1 lists the values of uncertainty (k=2) of the instruments used in the experimental facility.

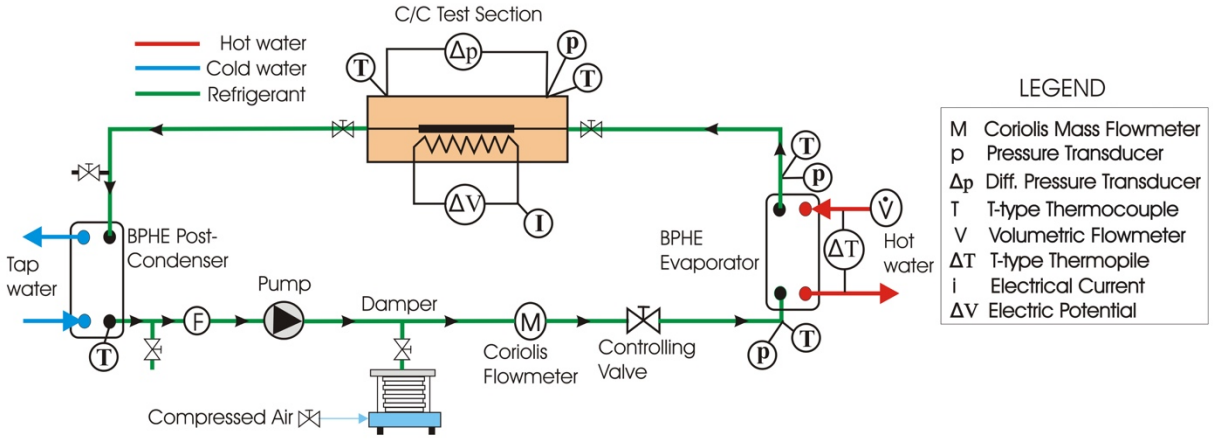

Figure 1: Schematic of the experimental setup.

Table 1: Instruments uncertainty.

Transducer	**Uncertainty (k=2)**
T-type thermocouples	± 0.1 K
T-type thermopiles	± 0.05 K
Electric power	± 0.26% of the reading
Coriolis mass flowmeter (refrigerant loop)	± 0.10% of the reading
Magnetic volumetric flowmeter (hot water loop)	±0.2% of FS=0.33 10^{-3} m^3/s
Differential pressure transducer (test section)	±0.075% of 0.3 MPa
Absolute pressure transducers	± 0.065% of FS=4 MPa

The test section consists of a 440x130x50 mm parallelepiped of low conductivity epoxy composite material, having a thermal conductivity around 0.25 W m^{-1} K^{-1} and showing high working temperature, which can reach 250 °C. The block was machined to obtain two plenums where the refrigerant enters and exits and where both the refrigerant temperature and pressure are measured by means of calibrated T-type thermocouples and high accuracy pressure transducers, respectively. A guide was milled in the center of the block to locate the Carbon/Carbon sample. A Ni-Cr wire resistance was used to heat the C/C sample from the bottom face. The heat was supplied by means of stabilized DC power supply, rated up to 900 W. The top wall consists of a 20 mm high tempered glass positioned over the test section; the sealing is accomplished using an EPDM o-ring located into a guide previously milled on the top of the test section block. Two stainless steel plates are located on the top and on the bottom of the assembled test section and they are bolted together.

3. CARBON/CARBON SAMPLE

Carbon fiber reinforced carbon matrix (C/C) composites have been widely used in aeronautics and aerospace industries for several decades (Fitzer and Manocha, 1998). As described by Delhaes (2003), the C/C composites are frequently fabricated by Chemical Vapor Infiltration (CVI) of porous carbon fiber preforms. This method was also applied to the present sample, which was obtained by CVI of a 3D preform, previously heated up to more than 1800 °C. The obtained C/C block was then re-heated to improve the thermal conductivity of the deposited carbon matrix. The thermal conductivity through the thickness was estimated by the manufactured to be 65 W m^{-1} K^{-1}.

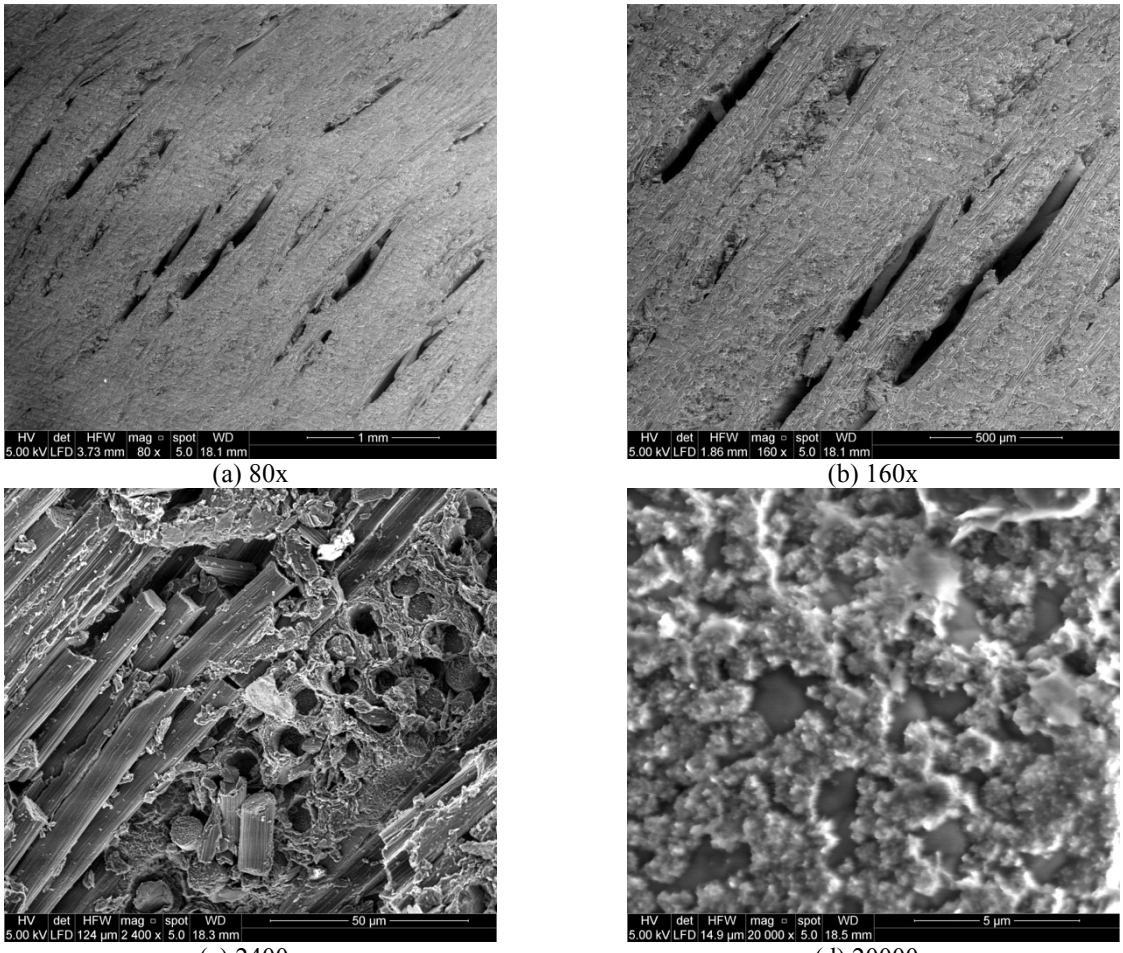

(a) 80x (b) 160x

(c) 2400x (d) 20000x

Figure 2: SEM images of the C/C sample.

The sample was obtained by machining the Carbon/Carbon block to realize a 180 mm long, 10 mm wide, and 20 mm thick plate. On lateral side walls, 18 holes (9 on each side), 5 mm deep, were drilled below the surface (distance between the probe and the top surface 0.5 mm) to monitor the wall temperature distribution by locating as many calibrated T-type thermocouples. On the bottom face, a guide was milled to install a calibrated Ni-Cr electrical wire resistance. The surface was scanned via SEM imaging to analyze its morphology; a few samples of the acquired images are reported in Figure 2. As clearly shown by the SEM images, the surface is characterized by the presence of deep valleys, stochastically distributed all over the surface, (a) and (b). When increasing the magnification (2400x), the 3D tailored texture appears and carbon fibers can be easily observed (c); by further zooming the surface (20000x), a quite uniform distribution of deposited carbon structures on the primary carbon fibers preform appears (d).
The surface roughness of the C/C sample was measured by means of a 3D optical profilometer and, according to ISO4287, it results R_a=2.44 μm and R_z=13.1 μm.
As highlighted in Figure 2, the C/C surface presents a non-uniform surface with several deep valleys; the surface can be considered partially hydrophilic. This property affects the boiling behavior of the surface during the flow boiling process; in fact, it was found that the boiling performance changed showing a hysteresis (Forrest *et al.,* 2010, Mancin *et al.,* 2015). It is well known that the hydrophilic behavior of a surface is directly correlated to the contact angle between the surface and a liquid droplet. For this reason, some preliminary tests were carried to measure the contact angle exhibited by distilled water droplets on C/C and on a reference copper surface.
As comprehensively described by Kwok and Neumann (1999), the contact angle measurement is still a tricky and rather difficult operation because it may be affected by several parameters: in particular, the droplet volume has a great influence on contact angle results. After a sensitivity analysis, 5 μL distilled water droplets were selected as reference volume for the contact angle measurements. The water droplets were deposited on the surface by means of a calibrated Hamilton syringe dispenser. The drop shape analysis was conducted using a free referenced plugin software for ImageJ (a general purpose free image-processing package) called "DropSnake" that is fully described in Stalder *et al.* (2006).
The mean measured contact angle with copper surface was equal to 87°±2°, while the one with C/C surface was equal to 67°±4° (at ambient temperature of 23°C); these results highlight a contact angle difference between C/C and copper surface around 20°, confirming the partial hydrophilicity of the C/C sample as compared to the reference copper surface.

3. DATA REDUCTION

As described in the previous section, the subcooled liquid pumped by the magnetically coupled gear pump is vaporized into a BPHE fed with hot water. Thus, the vapor quality at the inlet of the test section can be calculated from a thermal balance at the evaporator, as:

$$q_{evap} = \dot{m}_w \cdot c_{p,w} \cdot \left(t_{w,in} - t_{w,out}\right) = \dot{m}_r \cdot \left(J_{in,TS} - J_{L,sub}\right) \quad (1)$$

where $\dot{m}_w$ is the water mass flow rate, $c_{p,w}$ is the specific heat capacity of the water, $t_{w,in}$ and $t_{w,out}$ are the inlet and outlet water temperatures. The right-hand side term of eq. (1) reports the refrigerant side heat flow rate where $\dot{m}_r$ is the refrigerant mass flow rate while $J_{in,TS}$ and $J_{L,sub}$ are the unknown specific enthalpy at the inlet of the test section and the specific enthalpy of the subcooled liquid entering the BPHE, respectively. Once calculated $J_{in,TS}$, the vapor quality at the inlet of the test section can be estimated by:

$$x_{in,TS} = \frac{J_{in,TS} - J_L}{J_V - J_L} \quad (2)$$

where J_L and J_V are the specific enthalpies of the saturated liquid and vapor, respectively, evaluated at the saturation pressure of the refrigerant measured at the inlet of the test section.
Preliminary heat transfer measurements permitted to estimate the heat loss (q_{loss}) due to conduction through the test section as a function of the mean wall temperature. The tests were run under vacuum conditions on the refrigerant channel by supplying the power needed to maintain the mean wall temperature at a set value. The measurements were carried out by varying the mean wall temperature from 28 °C to around 60 °C. The results show that the heat loss increases linearly as the mean wall temperature increases (R>0.99). In the tested range of wall temperature, the heat loss by conduction through the test section can be estimated by:

$$|q_{loss}| = 0.3193 \cdot \bar{t}_{wall}[°C] - 7.0427 \quad [W] \quad (3)$$

thus, the actual heat flow rate q_{TS} supplied to the sample is given by:

$$q_{TS} = P_{EL} - |q_{loss}| = \Delta V \cdot I - |q_{loss}| \quad (4)$$

It is worth underlying that the q_{loss} varied from 2.5% to 4% of the electrical power supplied. The two-phase heat transfer coefficient *HTC*, referred to the base area A_{base}, can be defined as:

$$HTC = \frac{q_{TS}}{A_{base} \cdot (\bar{t}_{wall} - \bar{t}_{sat})} \quad (5)$$

where $\bar{t}_{wall}$ is the average value of the measured wall temperatures $t_{wall,i}$ as:

$$\bar{t}_{wall} = \frac{1}{18} \sum_{i=1}^{18} t_{wall,i} \quad (6)$$

where i-th value of wall temperature, $t_{wall,i}$, is calculated from the measured one accounting for the thermal resistance of the s=0.5 mm thick layer of C/C over each thermocouple; by assuming a 1-D conductive model, the i-th wall temperature is given by:

$$t_{wall,i} = t_{C/C} - \Delta t_{1-D} = t_{C/C} - \frac{s}{\lambda_{C/C}} \cdot HF \quad (7)$$

In this case, $\lambda_{C/C} = 65$ W m^{-1} K^{-1} and *HF* is the imposed heat flux. At *HF*=50 kW m^{-2}, the $\Delta t_{1\text{-}D}$ was equal to 0.40 K. The average value of the saturation temperatures $\bar{t}_{sat}$ is obtained from the measured values of the pressure:

$$\bar{t}_{sat} = \frac{t_{sat,in}(p_{sat,in}) + t_{sat,out}(p_{sat,out})}{2} \quad (8)$$

Thermodynamic and transport properties are estimated from RefProp v9.1 (Lemmon *et al.*, 2013). A detailed error analysis was performed in accordance with Kline and McClintock (1953) using the values of the uncertainty of the instruments listed in Table 1; it was estimated that the uncertainty (k=2) on the two-phase heat transfer coefficient showed a mean value of ±2.1% and a maximum value of ±3.8%, while the uncertainty on the vapor quality was ±0.03.

3. EXPERIMENTAL RESULTS

The experimental results were collected at 30 °C, which can be considered suitable for electronic thermal management. A hysteresis phenomenon is clearly visible in the results plotted in Figure 3, which presents the heat transfer coefficients obtained during flow boiling heat transfer of R134a at G=50 kg m^{-2} s^{-1} and *HF*=50 kW m^{-2}. The tests were run following a two step procedure: at first, the mean vapor quality was increased up to the dryout (x_{mean}=0.86) and then, it was decreased down to the initial value.

The activation process can be analyzed by starting from the black squares and following the black arrows, at x_{mean}=0.28 the heat transfer coefficient is slightly higher than 11000 W m^{-2} K^{-1} and then it quickly increases with vapor quality, being around 14400 W m^{-2} K^{-1}at x_{mean}=0.68.

A further increase of the vapor quality leads to the onset of the dryout, which occurs at x_{mean}=0.81. As the liquid fraction decreases (i.e. the vapor quality increases), the number of the activated nucleation sites increases and the surface undergoes to a continuous activation, which is then completed during the dryout when a thin vapor layer covers almost all the surface.

When decreasing the vapor quality down from x_{mean}=0.85 (grey circles), by following the red arrows, the dryout region recedes toward the end of the channel and the liquid is able to re-wet the surface which, now, remains activated. In fact, during the dryout a vapor layer covers the surface remaining trapped in the nucleation sites, which once rewetted by the liquid become activated. The new values of the heat transfer coefficient vary from 15100 W m^{-2} K^{-1} at x_{mean}=0.75 to 13700 W m^{-2} K^{-1} at x_{mean}=0.29, meaning that there is also a non-negligible effect of the convective boiling heat transfer mechanism. At low vapor quality, the new heat transfer coefficient is some 22% higher than that measured for the non-activated surface. Once the activation process is completed, the surface remains activated and if the operating conditions are changed, i.e. mass velocity and/or vapor quality are changed, the heat transfer performance does not vary anymore.

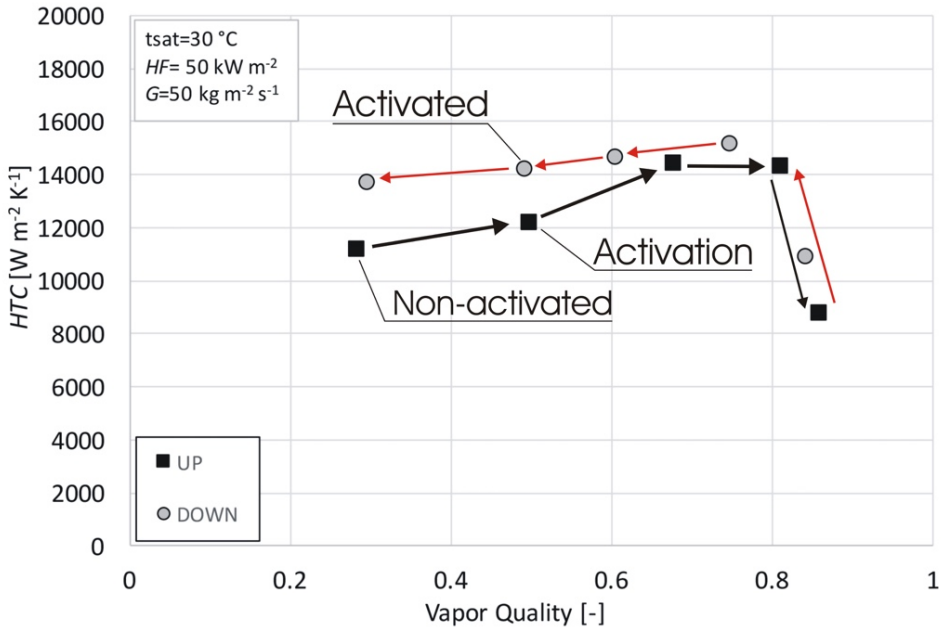

Figure 3: Flow boiling heat transfer coefficient vs. mean vapor quality: activation process.

The described phenomenon can be explained considering the wall superheating reported in Figure 4; at the beginning of the tests, at low vapor quality, when the surface is not activated, the wall superheat is higher than 4 K but, when increasing vapor quality, this value starts to continuously decrease before the onset of the dryout (x_{mean}=0.81), which implies a sudden increase of the wall temperature. When decreasing the vapor quality back to the initial value, the wall superheat becomes lower than that measured before, being always less than 4 K. Similar results were also observed and reported by Forrest *et al.* (2010) in the case of pool boiling for hydrophilic surfaces, which tend to delay the onset of the nucleate boiling because their high wettability limits the activation of the nucleation sites. In particular, Forrest *et al.* (2010) experimentally demonstrated that for the superhydrophilic wires, the high wettability leads to the majority of cavities being flooded at the start of each test, which, in turn, requires higher wall superheats for nucleation.

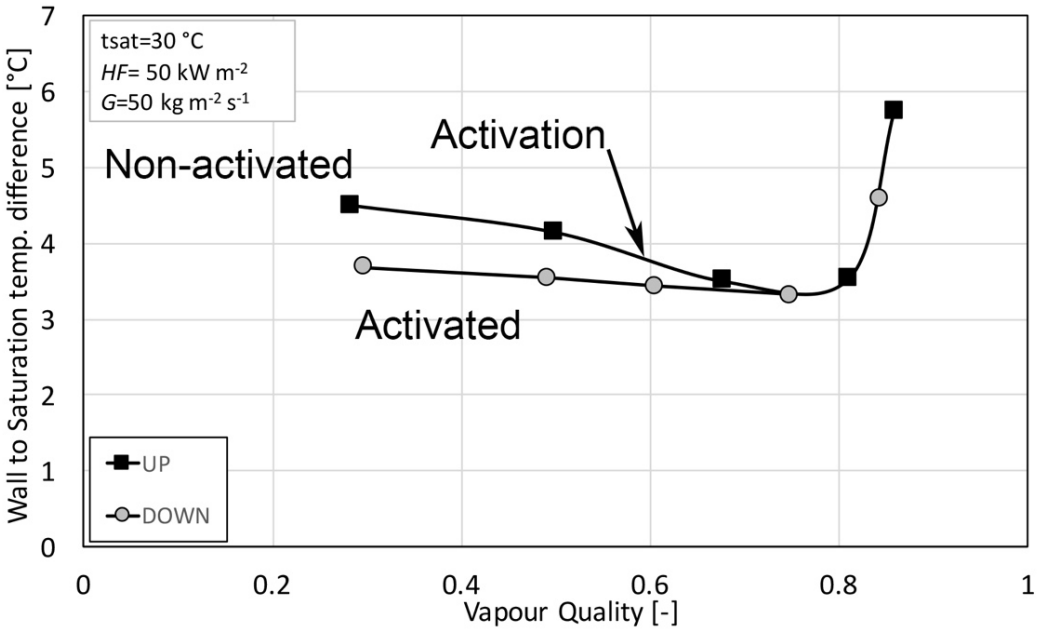

Figure 4: Wall-to-saturation temperature difference vs. mean vapor quality: activation process.

However, upon nucleation, vapor becomes entrapped in the cavities, lowering the required superheat. The Authors observed a hysteresis in the boiling curve due to the creation of entrapped vapor in cavities that became activated at high wall superheats. More recently, Mancin *et al.* (2015) found similar behavior in the case of refrigerant flow boiling on a microparticles coated copper surface; the Authors stated that the coating changed the wettability of the surface, which became hydrophilic and showed a similar hysteresis during the boiling process: once activated the coated surface exhibited 2.5 higher values of heat transfer coefficient. As also confirmed by the contact angle measurements, the C/C surface was found to be partially hydrophilic.

Figures 5, 6, and 7 present 7 flow visualization image sequences taken during R134a boiling tests at G=50 kg m^{-2} s^{-1} and HF=50 kW m^{-2}, which were also presented and discussed in Figures 3 and 4. In fact, the image sequences allow one to follow the activation process (Figure 5), up to the onset of the dryout (Figure 6), down to the lowest vapor quality with the activated surface (Figure 7). An interesting comparison can be drawn comparing four image sequences (II) and (III) of Figure 5 with (V) and (VI) of Figure 7; the images refer to vapor qualities around 0.7 and 0.5, respectively, and one can observe that, when the surface is activated (V) and (VI), a greater amount of detached bubbles is present in the two-phase mixture, meaning that a greater number of nucleation sites are activated. Considering the images reported in Figure 6 (IV), the partial dewetting phenomenon due to the incipient dryout is clearly visible; at these conditions, the heat transfer is still very high because the liquid continuously rewets the surface.

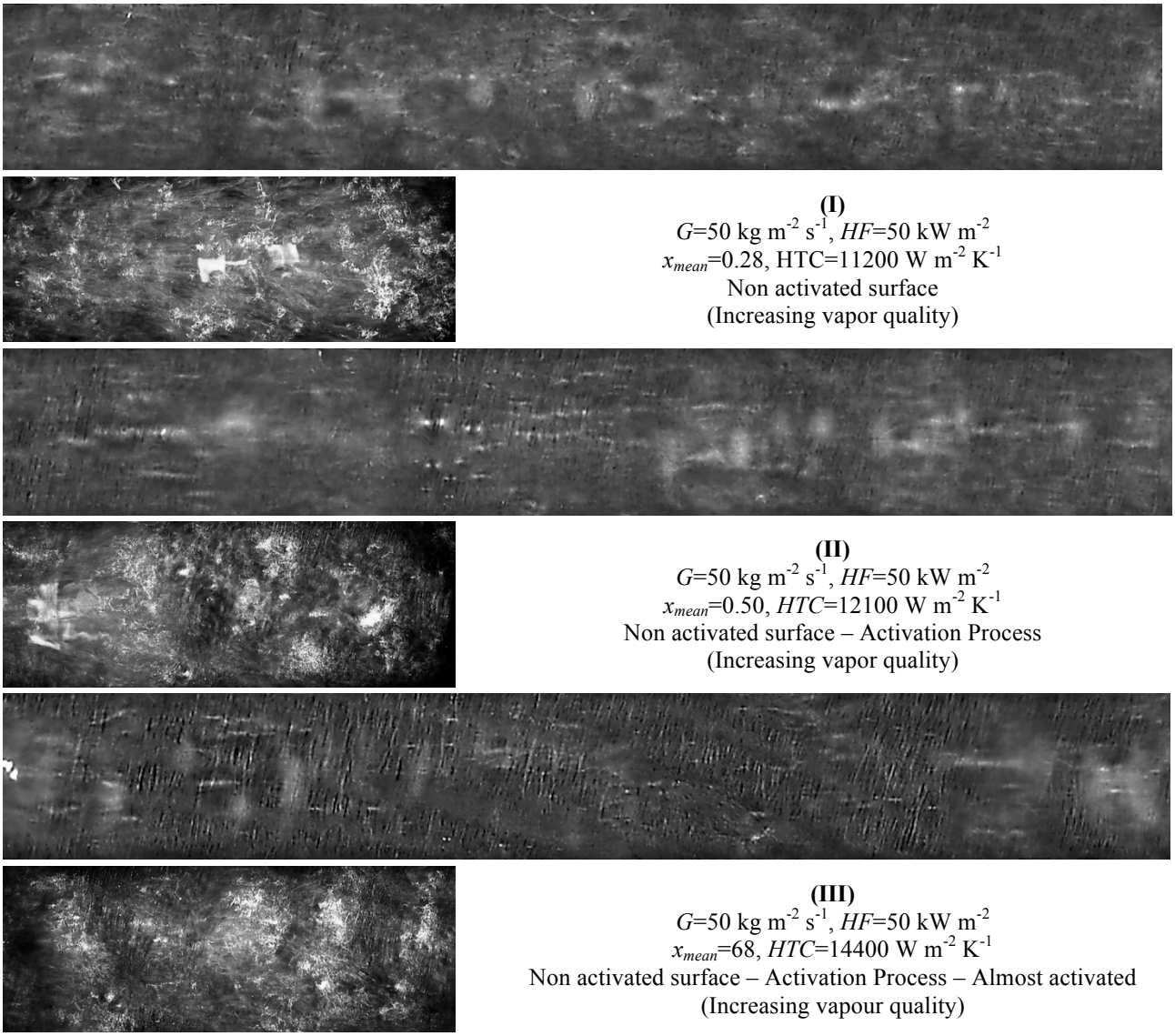

Figure 5: Flow boiling visualization referred to experimental measurements of Figure 3 (Activation process – black squares). Flow from left to right.

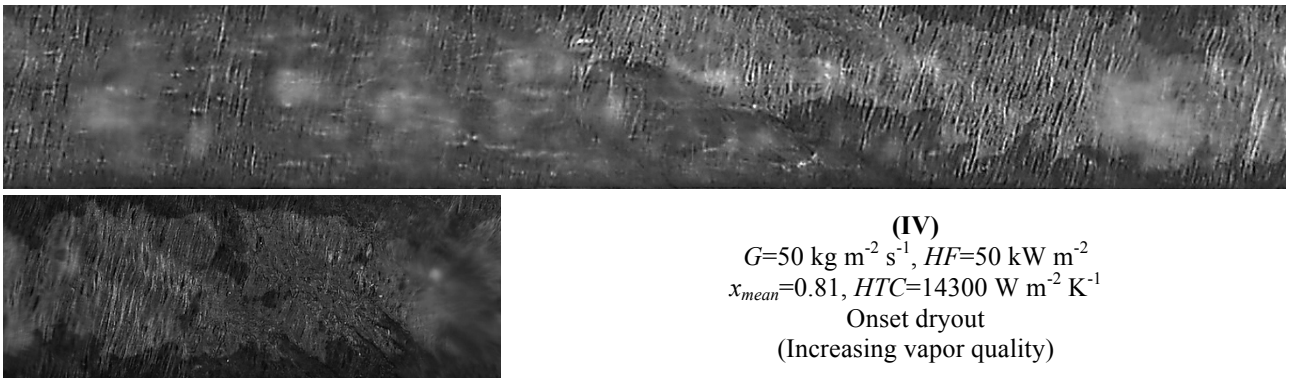

(IV)
G=50 kg m^{-2} s^{-1}, HF=50 kW m^{-2}
x_{mean}=0.81, HTC=14300 W m^{-2} K^{-1}
Onset dryout
(Increasing vapor quality)

Figure 6: Flow boiling visualization referred to experimental measurements of Figure 3 (Onset dryout). Flow from left to right.

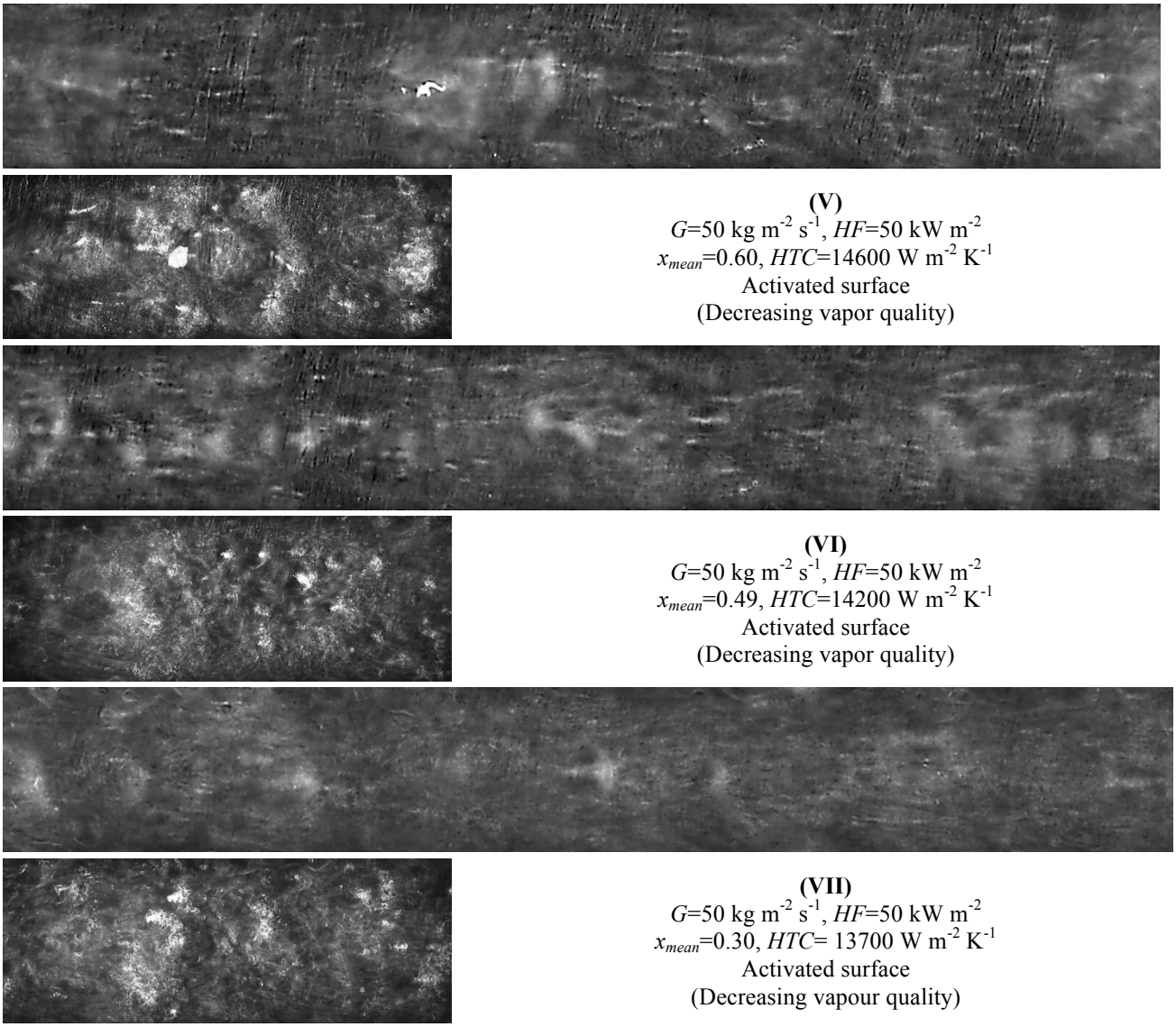

(V)
G=50 kg m^{-2} s^{-1}, HF=50 kW m^{-2}
x_{mean}=0.60, HTC=14600 W m^{-2} K^{-1}
Activated surface
(Decreasing vapor quality)

(VI)
G=50 kg m^{-2} s^{-1}, HF=50 kW m^{-2}
x_{mean}=0.49, HTC=14200 W m^{-2} K^{-1}
Activated surface
(Decreasing vapor quality)

(VII)
G=50 kg m^{-2} s^{-1}, HF=50 kW m^{-2}
x_{mean}=0.30, HTC= 13700 W m^{-2} K^{-1}
Activated surface
(Decreasing vapour quality)

Figure 7: Flow boiling visualization referred to experimental measurements of Figure 3 (grey circles). Flow from left to right.

Figure 8 reports the heat transfer coefficients measured during flow boiling of R134a on the C/C surface as a function of the mass velocity. For the sake of clarity, only the data collected after the end of the activation process of the C/C surface prior the onset of the dryout is plotted. From the analysis of the experimental results, it clearly appears that, for a given vapor quality, the heat transfer slightly increases when passing from G=50 kg m^{-2} s^{-1} to G=100 kg m^{-2} s^{-1}, while a further increase of the refrigerant mass flux up to G=200 kg m^{-2} s^{-1} does not lead to an improvement of the boiling performance and the heat transfer coefficients remain almost constant, even slightly lower especially at high vapor quality. This is mainly due to the non negligible two-phase pressure drop exhibited at G=200 kg m^{-2} s^{-1}, which penalizes the flow boiling heat transfer coefficients.

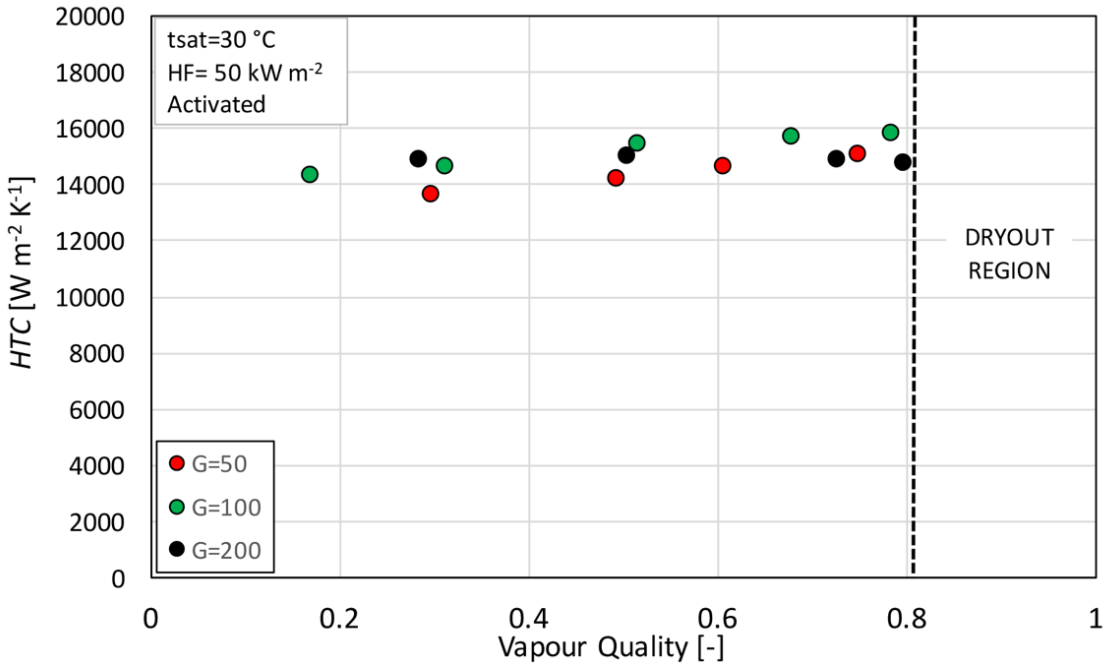

Figure 8: Flow boiling heat transfer coefficient vs. mean vapor quality for fully activated surface as a function of the mass velocity. G expressed in [kg m^{-2} s^{-1}]

4. CONCLUSIONS

This paper presents the experimental data collected during R134a flow boiling heat transfer on a Carbon/Carbon surface. The results show the peculiar heat transfer properties of this material; in particular, the experimental measurements highlight the presence of hysteresis in the boiling performance of the surface, which can be linked to its wettability characteristics. The experimental technique allowed for a detailed analysis of the activation process including also the two-phase flow visualization by means of a high speed camera.
In general, this material shows very interesting heat transfer capabilities during flow boiling, which makes it worth of future research investigation to better understand the underlying heat transfer mechanisms to maximize its boiling performance for possible future applications in compact, light, and smart heat sinks.

NOMENCLATURE

A	area	(m^2)
c_p	specific heat capacity	(J kg^{-1} K^{-1})
G	mass velocity	(kg m^{-2} s^{-1})
HTC	heat transfer coefficient	(W m^{-2}K^{-1})
HF	heat flux	(W m^{-2})
J	specific enthalpy	(J kg^{-1})
k	coverage factor	(-)
I	electrical current	(A)
$\dot{m}$	mass flow rate	(kg s^{-1})

p	pressure	(Pa)
P_{EL}	electrical power	(W)
q	heat flow rate	(W)
R	correlation index	(-)
s	thickness	(m)
t	temperature	(°C)
x	vapor quality	(-)
Δt	temperature difference	(°C)
ΔV	electric potential	(V)
λ	thermal conductivity	(W m^{-1} K^{-1})
Subscript		
1-D	1-dimension	
base	base area	
C/C	Carbon/Carbon	
evap	evaporator	
i	i-th	
in	inlet	
L	liquid	
loss	loss	
mean	mean	
out	outlet	
r	refrigerant	
sat	saturation	
sub	subcooled liquid	
TS	test section	
V	vapor	
w	water	
wall	wall	

REFERENCES

Ammerman, C.N., You, S.M., 2011, Enhancing small-channel convective boiling performance using a microporous surface coating, *J. Heat Transfer*, vol. 123: p. 976–983.

Carbon/Carbon Composites Project, 2009-2012, http://www.unh.edu/cc-composites/index.html

Chang, W.R., Chen, C.A., Ke, J.H., Lin, T.F., 2010, Subcooled flow boiling heat transfer and associate bubble characteristics of FC-72 on a heated micro-pin-finned silicon chip, *Int. J. Heat Mass Transfer,* Vol. 52: p. 5605–5621.

Delhaes, P., 2003, *Fibers and composites*, Taylor and Francis, New York.

Fitzer, E. Manocha, L.M., 1998, *Carbon reinforcements and carbon/carbon composites*, Berlin, Heidelberg, Springer.

Forrest, E., Williamson, E., Buongiorno, J., Hu, L.W., Rubner, M., Cohen, R., 2010. Augmentation of nucleate boiling heat transfer and critical heat flux using nanoparticle thin-film coatings. *Int. J. Heat Mass Transfer*, vol. 53: p. 58–67.

Khanikar, V., Mudawar, I., Fisher, T., 2009, Effects of carbon nanotube coating on flow boiling in a micro-channel, *Int. J. Heat Mass Transfer,* Vol. 52: p. 3805–3817.

Kline, S.J., McClintock, F.A., 1953. Describing uncertainties in single-sample experiments. *Mech.Eng*. 75, 3–8.

Kwok, D.Y., Neumann, A. W. 1999, Contact angle measurement and contact angle interpretation, *Advances in Colloid and Interface Science*, vol. 81: p. 167-249.

Lemmon, E.W., Huber, M.L., McLinden, M.O., 2013, NIST Standard Reference Database 23: Reference Fluid Thermodynamic and Transport Properties- REFPROP, Version 9.1, National Institute of Standards and Technology, Standard Reference Data Program, Gaithersburg.

Mancin, S., Diani, A., Vezzù, S., Rossetto, L., 2015, Flow Boiling Heat Transfer of R1234yf on a Microparticle Coated Copper Surface, *Proc. of. the 24th IIR International Congress of Refrigeration*, ICR 2015. August 16-22, 2015, Yokohama, JP.

Rainey, K.N., Li, G., You, S.M., 2011, Flow boiling heat transfer from plain and microporous coated surfaces in subcooled FC-72, *J. Heat Transfer*, vol. 123: p. 918–925.

Singh, N., Sathyamurthy, V., Peterson, W., Arendt, J., Banerjee, D., 2010, Flow boiling enhancement on a horizontal heater using carbon nanotube coatings, *Int. J. Heat Fluid Flow,* Vol. 31: p. 201–207.

Stalder, A.F., Kulik, G., Sage, D., Barbieri, L., Hoffmann, 2006, A Snake-Based Approach to Accurate Determination of Both Contact Points and Contact Angles, *Colloids and Surfaces A: Physicochemical and Engineering Aspects*, vol. 286, (1-3): p. 92-103.